Cluster approach to the structure of ^{240}Pu

T. M. Shneidman,[1,2,3,*] G. G. Adamian,[2] N. V. Antonenko,[2] R. V. Jolos,[2] and Shan-Gui Zhou[1,4]

[1]*State Key Laboratory of Theoretical Physics, Institute of Theoretical Physics, Chinese Academy of Sciences, Beijing 100190, China*

[2]*Bogoliubov Laboratory of Theoretical Physics, Joint Institute for Nuclear Research, Dubna 141980, Russia*

[3]*Kazan Federal University, Kazan 420008, Russia*

[4]*Center of Theoretical Nuclear Physics, National Laboratory of Heavy Ion Accelerator, Lanzhou 730000, China*

(Received 30 June 2015; published 3 September 2015)

The cluster approach, which allows us to take into account both shape deformation parameters and cluster degrees of freedom, is developed to describe alternating-parity rotational bands. The important ingredient of the model is the dinuclear system concept in which the wave function of the nucleus is treated as a superposition of a mononucleus and two-cluster configurations. The model is applied to describe the multiple positive and negative parity rotational bands in ^{240}Pu. The observed excitation spectrum and the angular momentum dependences of the parity splitting and of the electric $E1$ and $E2$ transition moments are explained. Special emphasis is made on the investigation of the recently measured positive parity 0_2^+ rotational band of reflection-asymmetric nature. The results suggest that this band might be understood as being built on the lowest excited state in the mass asymmetry degree of freedom. The $B(E1)/B(E2)$ branching ratios between the reduced transition probabilities of decay from the states of the 0_2^+ band to the first negative parity band and to the groundstate band, respectively, are calculated and compared with experimental data.

DOI: 10.1103/PhysRevC.92.034302 PACS number(s): 21.10.Re, 21.60.Ev, 21.60.Gx, 27.90.+b

I. INTRODUCTION

One of the distinctive properties of low-energy spectra of actinides is an appearance of the negative parity states at energies lower than the two-quasiparticle limit. Since the first observation of negative parity states near the ground state [1,2], a large amount of experimental data has been accumulated. An extensive review of experimental and theoretical achievements can be found in Refs. [3,4]. The lowest negative parity states form the rotational or quasivibrational bands which mainly decay via collective $E1$ transitions into the ground-state band. This picture has been understood as the possibility of strong reflection-asymmetric correlations in the vicinity of the ground state [5,6]. These correlations can be microscopically associated with the appearance of orbital pairs with $\Delta j = \Delta l = 3$ near the Fermi surface. Besides the actinides, a similar situation occurs in nuclei with masses near $A \sim 56$ and $A \sim 134$ (rare-earth mass region) that is in agreement with the experimental data. The results of calculations within the shell-corrected liquid drop models [7,8] and mean-field models [9–11] show that nuclei in these mass regions are either soft with respect to the octupole deformation or even octupole-deformed.

An alternative explanation is suggested by the cluster approach in which long-range multipole correlations might lead to the formation of light clusters on the surface of a heavy nucleus. The contribution of such bicluster configurations to the nuclear wave function naturally leads to an appearance of a reflection-asymmetric deformation. The strength of this deformation is determined by the relative weight of the bicluster configuration. Although well established for light nuclei [12], the justification of the cluster approach to the description of the structure of heavy nuclei is cumbersome. However, there exists evidence which supports the idea of clustering. First of all, the nuclei whose spectra exhibit the strong reflection-asymmetric correlations are good α emitters. Thus, there is a significant probability to form an α cluster in the surface region of the nucleus. It is also known from the Nillson-Strutinsky-type calculations for light nuclei that nuclear configurations corresponding to the minima of the potential energy contain particular symmetries which are related to certain cluster structures [13,14]. Several calculations performed for heavy nuclei [15–17] have shown that configurations with large quadrupole deformations and low-lying collective negative parity states are strongly related to clustering. The potential energies of cluster configurations with an α particle are close to or even lower than the binding energies for these nuclei [18]. Therefore, bicluster configurations with an α particle are expected to be important in the structure of actinides.

The idea of clustering has been used to describe the excitation spectra of actinides and rare-earth elements [18–26]. In the algebraic model [19–22], the corresponding wave functions of the ground and excited states consist of the components without and with dipole bosons in addition to the quadrupole bosons, which are related to mononucleus and alpha-cluster components, respectively. In Refs. [23,24], a cluster configuration with a lighter cluster heavier than ^{4}He was used in order to describe the properties of the low-lying positive and negative parity states. Within the cluster approach of the dinuclear system (DNS) model [18,25,26] the existing experimental data on the angular-momentum dependence of the parity splitting in the excitation spectra and the multipole transition moments ($E1$, $E2$, $E3$) of the low-lying alternating-parity states are well described in odd and even actinides $^{220-228}$Ra, ^{223,225,227}Ac, $^{222-232}$Th, ^{231}Pa, $^{232-238}$U, and ^{240,242}Po, and medium mass nuclei ^{144,146,148}Ba, ^{151,153}Pm, ^{146,148}Ce, ^{153,155}Eu, and ^{146,148}Nd.

*shneyd@theor.jinr.ru

As found in the recent experimental study of short-living Ra and Rn isotopes [27], the strength of $E3$ transitions opposes the trend predicted by the cluster model [18,25,26]. The reason for this disagreement is related to the disregard of the relative rotation of the DNS nuclei that is an oversimplification in the case of light Ra isotopes. The structure of the wave functions of the ground-state band and lowest negative parity states change drastically in nuclei with small or almost zero quadrupole deformation.

In Refs. [18,25,26], only the lowest negative parity bands ($K^\pi = 0^-$) have been considered. However, there is experimental evidence of negative parity collective states with $K \neq 0$ [28]. The structure of the positive parity bands seems to be strongly influenced by reflection-asymmetric deformation. In the recent experiment [29], the positive parity band built upon excited 0_2^+ state has been measured up to high spins in ^{240}Pu. Moreover, the reduced transition probabilities from this band to the lowest negative parity band have been observed. The collective character of these transitions shows a significant contribution of the reflection-asymmetric degree of freedom. The abundant experimental information on the $E1$ transition rates between the members of the first negative parity band and ground-state band [30–32] and the recent results on ^{240}Pu [29] require theoretical analysis.

The description of the multiband structure of the excitation spectra of heavy nuclei is a difficult task in the frame of the microscopic models. So, it is useful to develop the semiphenomenological models which are based on the introduction of the collective coordinates related to the violation of the reflection symmetry. Based on a microscopic understanding of the nature of the reflection-asymmetric deformation, the phenomenological models can be divided in two groups: the models with the quadrupole-octupole collective Hamiltonian [33,34] and the models with cluster degrees of freedom. One can also mention the approaches based on the interacting boson model [19–22] and based on the idea of aligned octupole phonons [35,36].

This work is devoted to the development of the phenomenological cluster approach which is based on the assumption that the intrinsic nuclear wave function can be taken as a superposition of the mononucleus and various bicluster configurations. The interaction between the degrees of freedom describing the motion of the clusters causes the complex multiband structure in the nuclear excitation spectrum. The most important degree of freedom is the mass asymmetry. The nuclear wave function in the mass asymmetry coordinate determines the relative weight of the cluster components and, thus, the strength of reflection-asymmetric deformation. It is worth noting that in the frame of this approach the 0_2^+ state, measured in ^{240}Pu, is simply described as an excited state in the mass asymmetry degree of freedom. In Ref. [37], we applied a similar approach to treat the properties of ^{220}Th, which has a strong reflection-asymmetric deformation and relatively small quadrupole deformation [38]. The present aim is to treat the situation when the nucleus, ^{240}Pu, has both strong quadrupole and strong reflection-asymmetric deformations.

The paper is organized as follows. In Sec. II the theoretical background is presented. The parameters of the Hamiltonian are derived with the DNS model in Sec. III. Section IV is devoted to the application of the model to the structure and electromagnetic transitions in ^{240}Pu.

II. MODEL

A. The Hamiltonian

Instead of parametrization of the nuclear shape in terms of multipole deformation parameters [39,40], we use the degrees of freedom related to the DNS or cluster system [41]. The DNS is understood as the system of two nuclei (A_1, Z_1) and (A_2, Z_2) kept together in touching configuration by the nucleus-nucleus potential. As a mononucleus, we consider a unified nuclear system with charge $Z_1 + Z_2 = Z$ and atomic number $A_1 + A_2 = A$. The degrees of freedom describing the collective excitations are related to the rotation of the DNS as a whole, to the relative motion of the DNS fragments, to the intrinsic excitations of the fragments, and to the transfer of nucleons between the DNS fragments. The latter process is described here with mass asymmetry $\xi = A_2/A$ and charge asymmetry $\xi_Z = Z_2/Z$ coordinates. The values of $\xi = 0$ or $\xi = 1$ correspond to the mononucleus configurations ($A_1 = A, A_2 = 0$) or ($A_1 = 0, A_2 = A$), respectively.

The motion in ξ destroys the reflection-symmetric shape of the nuclear system. The main idea of our approach is that the intrinsic nuclear wave function can be described as a superposition of the mononucleus and different dinuclear configurations, which are realized with certain probabilities. The mononucleus is taken to be quadrupole deformed. The mass asymmetry ξ is described as a continuous variable.

We presume that the main source of the reflection-asymmetric deformation is the contribution of the DNS $|\alpha\rangle \times |(A-4, Z-2)\rangle$ with an α particle as a light cluster. This idea is supported by the observation that the actinides are good α emitters. Thus, there is a significant probability to form an α cluster in the surface region of the nucleus. Moreover, our calculations show that the potential energy of a DNS with an α cluster ($\xi = \xi_\alpha$) is close to or even lower than the binding energy for these nuclei, while the energies of configurations with a light cluster heavier than an α rapidly increase with ξ [18]. Therefore, in order to treat the ground-state properties of actinides, one can consider the region of mass asymmetry in the vicinity of the mononucleus and α-cluster DNS configuration. The contribution of the configurations with $\xi > \xi_\alpha$ are negligibly small.

In the region of interest, the dinuclear systems, which are produced by the motion in mass asymmetry, consist of a light spherical fragment (A_2, Z_2) and a heavy deformed (with an axially symmetric quadrupole deformation $\beta_{20} = \beta_0$) or spherical fragment (A_1, Z_1). In addition to the motion in ξ, we consider the relative rotation of the DNS fragments, described by the angles $\Omega_R = (\theta_R, \phi_R)$, and rotation of the heavy fragment, described by the angles $\Omega_h = (\theta_h, \phi_h)$. Angles (θ_R, ϕ_R) and (θ_h, ϕ_h) are measured in the laboratory system (Fig. 1). One can introduce the plain angle ϵ between the symmetry axis of the heavy fragment and the vector of the relative distance $\mathbf{R}$. The classical expression for the kinetic energy of the system with the chosen degrees of freedom is written as a sum of terms describing the motion in mass asymmetry, relative rotation of the DNS fragments, and

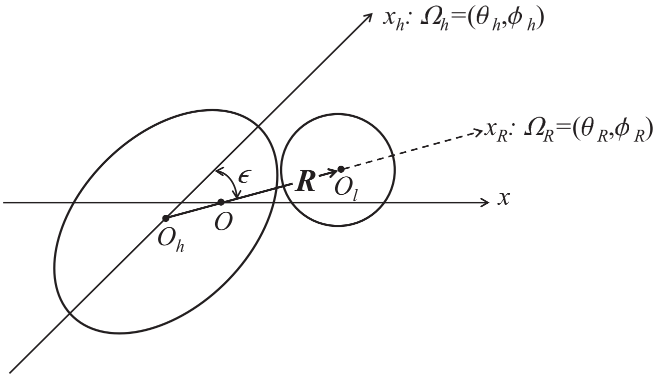

FIG. 1. The schematic picture of the dinuclear system with the indicated degrees of freedom used. The orientation of the vector **R** connecting the centers of nuclei is defined by the angles $\Omega_R = (\theta_R,\theta_R)$ in the laboratory frame Ox_R. The orientation of the intrinsic coordinate system $O_h x_h$ related to the quadrupole deformed heavy fragment is defined by the angles $\Omega_h = (\theta_h,\phi_h)$.

rotation of the heavy fragment:

$$T = \tfrac{1}{2}B(\xi)\dot{\xi}^2 + \tfrac{1}{2}\mu(\xi)R_{\mathrm{m}}^2(\xi)\big(\dot{\theta}_R^2 + \theta_R^2\dot{\phi}_R^2\big) + \Im_h(\xi)\big(\dot{\theta}_h^2 + \theta_h^2\dot{\phi}_h^2\big). \tag{1}$$

Here, $\mu = m_0\frac{A_1A_2}{A} \approx m_0A\xi$ is the reduced mass of the nuclear system ($\xi \ll 1$) where m_0 is the nucleon mass. The value of the relative distance $R = R_{\mathrm{m}}$ corresponds to the touching configuration for a certain value of ξ. The quantities $B(\xi)$ and $\Im_h(\xi)$ are the effective mass for the motion in mass asymmetry and the moment of inertia of the heavy fragment (or mononucleus). The method of calculation of $B(\xi)$ is described in Ref. [42]. In this work, however, we replace the effective mass parameter for the motion in mass asymmetry by its value $B(\xi_0)$ at average mass asymmetry ξ_0, $0 < \xi_0 < \xi_\alpha$:

$$B(\xi) = B(\xi_0). \tag{2}$$

The value $B(\xi_0) = B$ is then treated as a parameter of the model. In our calculation we take $B(\xi_0) = 14 \times 10^5 m_0$ fm^2. This value is larger than the one used in our previous calculations [18,26] because the additional degrees of freedom considered here result in the renormalization of the mass tensor. In Ref. [37], a similar value of B was used to describe the excitation spectra in ^{220}Th.

Because $\xi \ll 1$, in the quantization of expression (1) we leave only the terms of the lowest order in ξ. As a result, the following expression is obtained for the quantum kinetic energy operator:

$$T = -\frac{\hbar^2}{2B}\frac{1}{\xi}\frac{\partial}{\partial\xi}\xi\frac{\partial}{\partial\xi} + \frac{\hbar^2}{2\mu(\xi)R_{\mathrm{m}}^2(\xi)}L_R^2 + \frac{\hbar^2}{2\Im_h(\xi)}L_h^2, \tag{3}$$

where the angular momentum operators have the form

$$L_i^2 = -\frac{1}{\sin\theta_i}\frac{\partial}{\partial\theta_i}\sin\theta_i\frac{\partial}{\partial\theta_i} - \frac{1}{\sin^2\theta_i}\frac{\partial^2}{\partial\phi_i^2} \quad (i = R,h). \tag{4}$$

The potential energy of a nuclear system with mass asymmetry ξ is written as

$$U(\xi,\epsilon) = U_0(\xi) + U_\epsilon(\xi)\sin^2\epsilon, \tag{5}$$

where ϵ is related to Ω_R and Ω_h by the expression

$$\sin^2\epsilon = \frac{2}{3}\left(1 - \frac{4\pi}{\sqrt{5}}[Y_2(\Omega_h)\times Y_2(\Omega_R)]_{00}\right). \tag{6}$$

The dependence of the potential on ϵ is approximated by the second-order expansion. In (5), the potential energy has a minimum which corresponds to the pole-to-pole orientation ($\epsilon = 0$).

Using Eqs. (3) and (5) for the kinetic and potential energies, respectively, and the expression (6) we obtain the Hamiltonian of the model in the form

$$\begin{aligned} H &= H_\xi + H_{\mathrm{rot}} + V_{\mathrm{int}}(\xi,\Omega_R,\Omega_h),\\ H_\xi &= -\frac{\hbar^2}{2B}\frac{1}{\xi}\frac{\partial}{\partial\xi}\xi\frac{\partial}{\partial\xi} + U_0(\xi) + \frac{2}{3}U_\epsilon(\xi),\\ H_{\mathrm{rot}} &= \frac{\hbar^2}{2\mu(\xi)R_{\mathrm{m}}^2(\xi)}L_R^2 + \frac{\hbar^2}{2\Im_h(\xi)}L_h^2,\\ V_{\mathrm{int}}(\xi,\Omega_R,\Omega_h) &= -\frac{8\pi}{3\sqrt{5}}U_\epsilon(\xi)\{Y_2(\Omega_h)\times Y_2(\Omega_R)\}_{00}, \end{aligned} \tag{7}$$

where H_ξ describes the motion in mass asymmetry, H_{rot} describes the rotational motion of the heavy fragment and the relative rotation of the fragments, and V_{int} describes the interaction between the rotational degrees of freedom.

B. Wave functions and symmetries

The Hamiltonian (7) is diagonalized on the set of basis functions

$$\Phi_{LM,\pi}^{l_1,l_2,n} = F_n(\xi)\big[Y_{l_1}(\Omega_h)\times Y_{l_2}(\Omega_R)\big]_{LM}, \tag{8}$$

where $n = 0,1,2,\ldots$, $l_1 = 0,2,4,\ldots$, $l_2 = 0,1,2,\ldots$. Because the heavy fragment is assumed by the axially symmetric quadrupole rotator, the quantum number l_1 can take only even values. Thus, the wave function does not change under the transformation $\theta_h \to \pi - \theta_h, \phi_h \to \pi + \phi_h$. The angular part of the wave function (8) is given by the bipolar spherical harmonics which provide the proper transformation with respect to the rotation and space inversion. The parity of the state is then determined as $\pi = (-1)^{l_2}$.

C. Multipole moments

The reduced transition probability for the transition from the initial state $|i\rangle$ to the final state $|f\rangle$ is calculated as

$$B(E\lambda; i \to f) = \frac{1}{2I_i + 1}|\langle f\|Q_\lambda\|i\rangle|^2, \tag{9}$$

where the multipole operator $Q_{\lambda\mu}$ is defined as

$$Q_{\lambda\mu} = \int \rho_Z(\mathbf{r})r^\lambda Y_{\lambda\mu}(\Omega)d\mathbf{r}. \tag{10}$$

To obtain the expression for the multipole operator in the DNS, we substitute the charge density operator $\rho_Z(\mathbf{r})$ into (10) by

$$\rho_Z(\mathbf{r}) = \rho_{Z_1}(\mathbf{r}) + \rho_{Z_2}(\mathbf{r}), \tag{11}$$

where $\rho_{Z_i}(\mathbf{r})$ $(i = 1,2)$ are the charge densities of the DNS fragments. Using (11), we rewrite the expression of the electric multipole moments for the DNS as

$$Q_{\lambda\mu} = \sum_{\lambda_1,\lambda_1+\lambda_2=\lambda} \sqrt{\frac{4\pi(2\lambda+1)!}{(2\lambda_1+1)!(2\lambda_2+1)!}} q_{\lambda_1\lambda_2}(\xi) \times \left\{Y_{\lambda_1}(\Omega_h)\times Y_{\lambda_2}(\Omega_R)\right\}_{\lambda\mu}, \quad (12)$$

where

$$q_{\lambda_1\lambda_2} = \sqrt{\frac{4\pi}{2\lambda_1+1}}\left[\left(\frac{A_1}{A}\right)^{\lambda_2} Q^{(2)}_{\lambda_1} + (-1)^{\lambda_2}\left(\frac{A_2}{A}\right)^{\lambda_2} Q^{(1)}_{\lambda_1}\right] R^{\lambda_2}. \quad (13)$$

Here, $Q^{(i)}_{\lambda}$ $(i = 1,2)$ are the intrinsic multipole operators of the DNS fragments. Because we assume that the light fragment (A_2,Z_2) is spherical and cannot be excited in the considered energy range, the only nonzero moment for it is $Q^{(2)}_0 = Z_2/\sqrt{4\pi}$. The heavy fragment is quadrupole deformed and has nonzero moments: $Q^{(1)}_0 = Z_1/\sqrt{4\pi}$ and $Q^{(1)}_2 = Q_0 \approx \frac{3Z_1R^2_{01}}{4\pi}\beta_0$.

The explicit expressions for the dipole, quadrupole, and octupole operators of the DNS are written in the form

$$\begin{aligned} Q_{1\mu} &= \epsilon_1\sqrt{4\pi}\frac{A_1Z_2 - A_2Z_1}{A} R\{Y_0(\Omega_h)\times Y_1(\Omega_R)\}_{1\mu},\\ Q_{2\mu} &= \epsilon_2\sqrt{4\pi}\frac{A_1^2Z_2 + A_2^2Z_1}{A^2} R^2\{Y_0(\Omega_h)\times Y_2(\Omega_R)\}_{2\mu}\\ &\quad + \frac{4\pi}{\sqrt{5}}Q_0\{Y_2(\Omega_h)\times Y_0(\Omega_R)\}_{2\mu}, \qquad (14)\\ Q_{3\mu} &= \epsilon_3\sqrt{4\pi}\frac{A_1^3Z_2 - A_2^3Z_1}{A^3} R^3\{Y_0(\Omega_h)\times Y_3(\Omega_R)\}_{3\mu}\\ &\quad - 4\pi\sqrt{\frac{7}{5}}Q_0\frac{A_2}{A}R\{Y_2(\Omega_h)\times Y_1(\Omega_R)\}_{3\mu}, \end{aligned}$$

where ϵ_i $(i = 1,2,3)$ are the effective charges introduced for dipole, quadrupole, and octupole transitions.

III. DEFINITION OF PARAMETERS WITH THE DINUCLEAR SYSTEM MODEL

The collective model with Hamiltonian (7) considers the motion in mass asymmetry in addition to the rotational motion. The ingredients of the Hamiltonian, such as potential energy functions $U_0(\xi)$ and $U_\epsilon(\xi)$, effective mass parameter $B(\xi_0)$, and the moment of inertia of the heavy fragment $\Im(\xi)$ can be treated as parameters or calculated with the DNS model.

To find $U_0(\xi)$ and $U_\epsilon(\xi)$, we use the following method. For a DNS with an α particle and Li as light fragments, we calculate the potential energy (5) as

$$U(\xi_i,\epsilon) = B_1(\xi_i) + B_2(\xi_i) + V(R = R_{\mathrm{m}}(\epsilon),\beta_0,\xi_i,\epsilon) + \frac{\hbar\omega_R(\xi_i)}{2} \quad (i = \alpha,\mathrm{Li}). \quad (15)$$

Here, B_1 and B_2 are the binding energies of the fragments. The experimental ground-state masses [43], if available, are used in the calculations. If not, the predictions of [44] are used. The shell effects and pairing correlations are included in the binding energies.

The nucleus-nucleus potential

$$V(R,\xi,\beta_0,\epsilon) = V_{\mathrm{C}}(R,\xi,\beta_0,\epsilon) + V_{\mathrm{N}}(R,\xi,\beta_0,\epsilon) \quad (16)$$

in (15) is the sum of the Coulomb potential

$$V_{\mathrm{C}}(R,\xi,\beta_0,\epsilon) = \frac{e^2Z_1Z_2}{R} + \frac{3}{5}\frac{e^2Z_1Z_2R^2_{01}}{R^3}\beta_0Y_{20}(\epsilon,0) + \cdots \quad (17)$$

and the nuclear interaction potential

$$V_{\mathrm{N}}(R,\xi,\beta_0,\epsilon) = \int \rho_1(\mathbf{r_1})\rho_1(\mathbf{R}_{\mathrm{m}} - \mathbf{r_2})F(\mathbf{r_1}-\mathbf{r_2})d\mathbf{r_1}d\mathbf{r_2}, \quad (18)$$

where $F(\mathbf{r_1}-\mathbf{r_2})$ is the Skyrme-type density dependent effective nucleon-nucleon interaction, known as the Migdal forces [45]. The nucleon densities ρ_i are approximated by Fermi distributions with the radius parameter $r_0 = 1.15$ fm for heavy fragments and $r_0 = 1.0$ fm for light (^{4}He, ^{7}Li) fragments. The diffuseness parameter of the density distribution of a light cluster is taken as 0.48 fm. For heavy cluster, we set $a = 0.56\sqrt{B^{(0)}_n/B_n}$ where $B^{(0)}_n$ and B_n are the neutron binding energies of the studied nucleus and of the heaviest isotope of the considered element. The details of calculations are presented in Refs. [18,46].

The nucleus–nucleus potential in (15) is calculated at $R = R_{\mathrm{m}}$ that corresponds to the minimum of the potential pocket in relative distance coordinate R [46]. The last term in (15) represents the energy of zero point vibration in this pocket. In agreement with the assumption (5), the potential energy (15) as a function of relative orientation of the fragments has a minimum which corresponds to the pole-to-pole orientation ($\epsilon = 0$).

The values U_α and U_{Li} calculated with Eq. (15) are used to interpolate the ξ dependence of the potential energy smoothly by the polynomial. The value of the potential energy $U_0(\xi = 0)$ for the mononucleus configuration, which is also required for the interpolation, is fitted to reproduce the value of the nuclear binding energy corresponding to the lowest eigenstate. To parametrize the angular dependence in (5), we set $U_\epsilon(\xi) = C\xi/2$ and fix the value of C by fitting the ϵ dependence of the potential energy of the α-particle DNS.

For the potential energy of the α and Li DNS, the calculations give $U(\xi_\alpha,\epsilon = 0) = 2.58$ MeV and $U(\xi_{\mathrm{Li}},\epsilon = 0) = 20.05$ MeV, respectively. The values of $\hbar\omega_R(\xi_\alpha,\epsilon) = 6.02$ MeV and $\hbar\omega_R(\xi_{\mathrm{Li}},\epsilon) = 4.85$ MeV are calculated by solving the Schrödinger equation in R in the potential pocket around $R = R_{\mathrm{m}}(\epsilon)$, for each value of angle ϵ. For simplicity, the potential pocket in the vicinity of the $R = R_{\mathrm{m}}$ is fitted by the Morse potential. As found, the dependence of the $\hbar\omega_R$ on ϵ is rather weak. For example, for the α-particle DNS, when ϵ varies from 0 to $\pi/2$, the frequency $\hbar\omega_R$ increases by only 220 keV. The calculated angular dependence of the energy of the α-particle DNS is shown in Fig. 2. Fitting this dependence with the expression (5), we get $U_\epsilon(\xi) = 2.58$ MeV.

Another quantity required to determine the energy spectrum with the Hamiltonian (7) is the moment of inertia of the heavy fragment. As shown in Ref. [17], the highly deformed states are well described, as the cluster systems and their moments of inertia are about 85% of the rigid-body limit. Microscopically

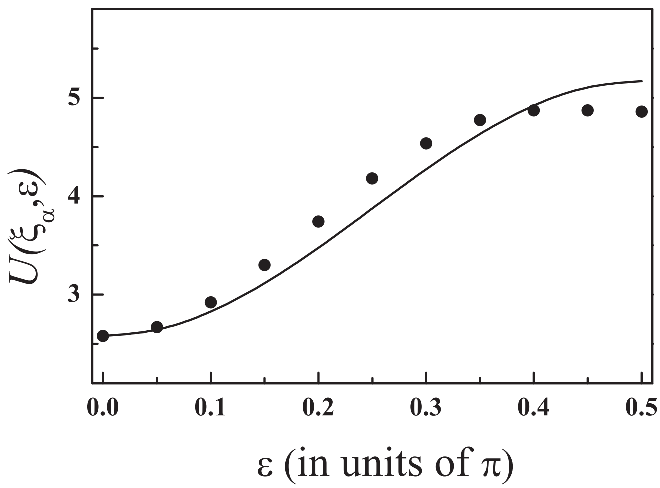

FIG. 2. Potential energy of the alpha-particle DNS as a function of angle ϵ. The values calculated with (15) are shown by dots. The line represents the fit of calculated points with the expression (5).

this effect can be related to the fact that the formation of the cluster in the surface region of the nucleus destroys the pairing correlations and leads to the increase in the moment of inertia. Thus, if we assume a pure cluster superposition (the weight of configurations with $\xi \leqslant \xi_\alpha$ is negligible) the moment of inertia of the heavy fragment must be taken as $\Im_h(\xi) = 0.85\Im_h^{(\mathrm{rig})}(\xi)$, where the rigid body moment of inertia $\Im_h^{(\mathrm{rig})}(\xi)$ is calculated with the deformation parameters from [43]. However, this procedure cannot be applied at $\xi < \xi_\alpha$. To overcome this difficulty, we assume the moment of inertia of the heavy fragment in the form

$$\Im_h(\xi) = c(\xi)\Im_h^{(\mathrm{rig})}(\xi), \tag{19}$$

where

$$c(\xi) = \begin{cases} 0.85, & \xi > \xi_\alpha, \\ c_0 + (0.85 - c_0)\frac{\xi}{\xi_\alpha}, & \xi < \xi_\alpha. \end{cases} \tag{20}$$

The quantity c_0 is a scaling parameter which is fixed by the calculation of the energy of the 2^+ state of the ground-state band. If the long spin bands are considered, the effect of centrifugal stretching must be included by adding smooth dependence of c_0 on I. In the calculation of the energy spectrum for ^{240}Pu presented below, the scaling parameter c_0 is taken in the form $c_0 = 0.42[1 + 4.8 \times 10^{-4} I(I+1)]$. So, the values of c_0 and $B(\xi_0)$ are the only parameters in our model which are not determined within the cluster approach. Other values are calculated and can be used for describing many nuclei. However, the value of $B(\xi_0)$ can be crudely estimated as in Ref. [42].

IV. CALCULATED RESULTS

A. Energy spectrum

The energy spectrum of ^{240}Pu, calculated by diagonalizing the Hamiltonian (7), is presented in Fig. 3. In the calculation we use the parameter set defined in the DNS approach (see Sec. III). One can see that the lowest excited states can be

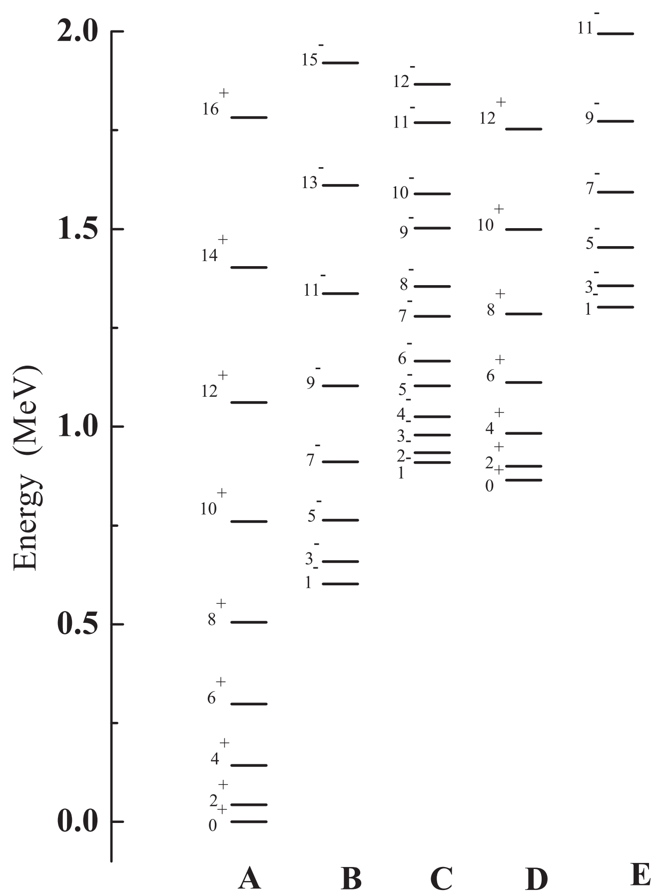

FIG. 3. Low-lying states of ^{240}Pu obtained by the diagonalization of the Hamiltonian (7). They can be gathered into the rotational bands marked as A, B, C, D, and E. Using the asymptotic solution for large angular momenta (see Appendix), the approximate value of quantum number K can be assigned to each band. For the bands A and D, we get $K^\pi = 0^+$, for the bands B and E, $K^\pi = 0^-$, and for the band C, $K^\pi = 1^-$.

gathered into the rotational bands, according to which basis function from the set (8) mostly contributes to the wave function of the state.

For the qualitative analysis of the structure of the spectrum, one can approximate the wave function by separating the motion in the mass asymmetry degree of freedom from the angular motion. Then we see that the rotational bands A, B, and C are built on the lowest state, whereas the bands D and E are built on the first excited state in the mass asymmetry coordinate. In this work, we are mainly interested in the structure and transitions involving states of bands A, B, and D. The results of calculations show that the wave functions of these bands, for not too large angular momentum, can be approximately written in the form

$$\begin{aligned} \Psi_{IM}^{A} &= \phi_0(\xi,I)\{\gamma_A(I)[I\times 0]_{IM} + \delta_A(I)[(I-2)\times 2]_{IM}\}, \\ \Psi_{IM}^{B} &= \phi_0(\xi,I)\{\gamma_B(I)[(I-1)\times 1]_{IM} \\ &\quad + \delta_B(I)[(I+1)\times 1]_{IM} + \epsilon_B(I)[(I-3)\times 3]_{IM}\}, \\ \Psi_{IM}^{D} &= \phi_1(\xi,I)\{\gamma_D(I)[I\times 0]_{IM} + \delta_D(I)[(I-2)\times 2]_{IM}\}, \end{aligned} \tag{21}$$

where $\phi_0(\xi,I)$ and $\phi_1(\xi,I)$ are the lowest and first excited states in the mass asymmetry coordinate, respectively. For the basis states in angular degrees of freedom, we use the shorthand notation

$$[l_1 \times l_2]_{IM} \equiv \left[Y_{l_1}(\Omega_h) \times Y_{l_2}(\Omega_R)\right]_{IM}. \tag{22}$$

The amplitudes $\gamma_i(I)$, $\delta_i(I)$, and $\epsilon_i(I)$, $(i = A,B,D)$ are the functions of angular momentum. At low angular momenta $\gamma_i(I) \gg \delta_i(I) \gg \epsilon_i(I)$. With increasing angular momentum, however, their values approach each other. In principle, Eqs. (21) can be used as a variational wave functions to find the approximate solutions of the Hamiltonian (7). This procedure is only valid for relatively small angular momenta. With increasing angular momenta more basis states start to contribute to the wave functions.

For the ground-state rotational band A, the angular part of the wave-function of the state with angular momentum I is roughly described by the function $[Y_{l_1=I}(\Omega_h) \times Y_{l_2=0}(\Omega_R)]_{IM}$. Because $\pi = (-1)^{l_2}$, the ground-state band contains only the states of positive parity with even angular momentum I. The wave functions of the lowest negative parity states of the band B have the dominant component $[Y_{l_1=I-1}(\Omega_h) \times Y_{l_2=1}(\Omega_R)]_{IM}$. They form a rotational band which contains the states of odd angular momentum and negative parity. This band can be interpreted as the $K^\pi = 0^-$ band. One should note that each eigenfunction of the Hamiltonian (7) is a superposition of the states with different K values and, thus, K can be considered as a quantum number only approximately. The next lowest band C of negative parity is formed from the states with the main contribution of $[Y_{l_1=I+1}(\Omega_h) \times Y_{l_2=1}(\Omega_0)]_{IM}$ component for odd angular momentum and $[Y_{l_1=I}(\Omega_h) \times Y_{l_2=1}(\Omega_0)]_{IM}$ component for even angular momentum. This band can be assigned to $K^\pi = 1^-$. In this case the angular momentum carried by the relative rotation is oppositely directed to the total angular momentum, thus shifting up the energy of this rotational band with respect to the 0^- band.

The first excited 0^+ state corresponds to the lowest excitation in the mass-asymmetry coordinate. Treating this 0^+ state similar to the ground state, all the constructions above can be repeated. So, the bands D and E are analogous to the bands A and B but built on the first excited state in ξ. This explanation of the nature of the excited reflection-asymmetric 0^+ band is different from that in Ref. [33], where it is considered as a two-octupole boson excited state. As seen in the Appendix, the chosen K values corresponds to the asymptotic quantum numbers of the bands for large angular momentum values, when the reflection-asymmetric deformation becomes stable and the rotational reflection-asymmetric bands are formed. So, the assignment of K values to the bands is quite justified.

Note that the spectrum given in Fig. 3 is typical for the quadrupole-deformed actinides [47]. The structure of the spectra changes for the actinides with small or almost zero quadrupole deformation (see, for example, ^{220}Th in Refs. [37,38]) because the relative rotation of the clusters starts to play a role. The disregard of this rotation in Ref. [18] causes the disagreement, which was pointed in Ref. [27], between the predictions and the recent measurement of the strength of $E3$ transitions in the light Ra and Rn isotopes.

The excitation spectra and the structure of the wave functions of the excited states strongly depend on the ratio of the frequency $\omega_h = \hbar^2/[2\Im(\bar{\xi})]$ of the rotation of heavy fragment to the frequency $\omega_R = \hbar^2/[2\mu(\bar{\xi})R_m^2(\bar{\xi})]$ of the relative rotation of the clusters. Here, $\bar{\xi}$ is the average mass asymmetry for a certain state. When the nucleus has strong quadrupole deformation, $\omega_h/\omega_R \ll 1$ and only a small fraction of the angular momenta contributes to the relative rotation. In this case, the states $[Y_{l_1=I\pm1}(\Omega_h) \times Y_{l_2=1}(\Omega_R)]_{IM}$ significantly contribute to the structure of the lowest negative parity states $[\gamma_B \gg \delta_B \gg \epsilon_B$ in Eqs. (21)]. For weakly deformed or transitional nuclei, $\omega_h/\omega_R \sim 1$ and the contribution of the state $[Y_{l_1=I-3}(\Omega_h) \times Y_{l_2=3}(\Omega_R)]_{IM}$ becomes important as well $(\gamma_B \sim \epsilon_B \gg \delta_B)$.

As seen from Eqs. (14), the expression for the octupole moment has two terms of opposite signs. The first term selects the basis states with $(\Delta l_1 = 0, \Delta l_2 = 3)$, whereas the second term selects the states with $(\Delta l_1 = 2, \Delta l_2 = 1)$. Because the amplitude ϵ_B is negligible for a strongly deformed nucleus, the first term of the operator $Q_{3\mu}$ gives almost no contribution to the octupole transition strength. In a weakly deformed nucleus, $\gamma_B \sim \epsilon_B$, and we expect that two terms of the operator $Q_{3\mu}$ negate each other and, thus, the strength of the octupole transition remains small. This qualitative discussion suggests that the recent experimental data on the strength of $E3$ transitions in the transitional and vibrational Ra and Rn isotopes [27] can be described in the frame of the model proposed. A detailed quantitative analysis with the proper intrinsic Hamiltonian for heavy fragments will be done in future.

The bands presented in Fig. 3 exhaust the lowest states of the Hamiltonian (7). All other solutions lie at sufficiently higher excitation energies. However, there are bands assigned to $K^\pi = 0^+$, 2^+, and 2^- which are absent in the calculated spectrum. The possible reason for this is that the present version of the model disregards the β and γ vibrations of the heavy fragment with stable axially symmetric quadrupole deformation. With these vibrations the calculated spectra of actinides would contain additional 0^+ and 2^+ rotational bands, built on the β and γ vibrational excitations, respectively. We can also expect the appearance of additional low-lying 0^- and 2^- bands, as a negative parity doublets to the β and γ vibrational bands. Note that the alternative explanation of the appearance of the low-lying 2^- bands in actinides is based on the concept of tetrahedral deformation [48,49].

The energies of the lowest rotational bands with the angular momentum up to $I = 30$ are given in Table I together with the available experimental data [32]. The agreement between the calculated and experimental excitation spectra is rather good for all rotational bands considered.

B. Parity splitting

The ground state band A and the first negative parity band B are usually treated as a unified alternating parity rotational band. In the case of stable reflection-asymmetric deformation, the alternating parity band contains positive and negative parity states, forming the smooth rotational band $0^+, 1^-, 2^+, 3^-, \ldots$. In actinides, however, the negative parity

TABLE I. Calculated (calc.) and experimental (exp.) energies of the members of the lowest positive and negative parity bands in ^{240}Pu. Experimental data are taken from Ref. [32].

Band *A*			Band *B*			Band *C*			Band *D*		
I	calc. (MeV)	exp.	*I*	calc. (MeV)	exp.	*I*	calc. (MeV)	exp.	*I*	calc. (MeV)	exp.
0^+	0.000	0.000	1^-	0.602	0.597	1^-	0.909	0.938	0^+	0.865	0.861
2^+	0.043	0.043	3^-	0.659	0.649	2^-	0.934	0.959	2^+	0.900	0.900
4^+	0.143	0.142	5^-	0.763	0.742	3^-	0.979	1.002	4^+	0.983	0.992
6^+	0.298	0.294	7^-	0.911	0.878	4^-	1.025	1.038	6^+	1.112	1.138
8^+	0.505	0.497	9^-	1.103	1.057	5^-	1.103	1.116	8^+	1.285	1.323
10^+	0.760	0.747	11^-	1.327	1.278	6^-	1.166	1.162	10^+	1.499	1.557
12^+	1.061	1.041	13^-	1.610	1.540	7^-	1.279		12^+	1.753	1.830
14^+	1.403	1.375	15^-	1.920	1.842	8^-	1.355		14^+	2.044	2.137
16^+	1.782	1.746	17^-	2.264	2.183	9^-	1.502		16^+	2.369	2.475
18^+	2.194	2.152	19^-	2.641	2.561	10^-	1.589		18^+	2.726	2.837
20^+	2.636	2.590	21^-	3.048	2.974	11^-	1.769		20^+	3.114	3.218
22^+	3.105	3.060	23^-	3.484	3.421	12^-	1.866		22^+	3.532	3.627
24^+	3.599	3.559	25^-	3.947	3.901	13^-	2.075		24^+	3.979	4.064
26^+	4.115	4.086	27^-	4.439	4.411	14^-	2.182		26^+	4.454	4.531
28^+	4.652	4.639	29^-	4.958	4.950	15^-	2.416		28^+	4.963	5.030
30^+	5.210	5.220			5.512	16^-	2.535		30^+	5.505	5.559
					6.096	17^-	2.785				
						18^-	2.922				
						19^-	3.172				
						20^-	3.340				
						21^-	3.576				
						22^-	3.790				
						23^-	3.999				
						24^-	4.266				
						25^-	4.447				
						26^-	4.770				
						27^-	4.919				
						28^-	5.301				
						29^-	5.420				
						30^-	5.860				

states are shifted up with respect to their expected position. This shift is quantitatively described by means of the parity splitting defined as [50]

$$S(I^-) = E(I^-) - \frac{(I+1)E^+_{(I-1)} + I E^+_{(I+1)}}{2I+1}. \tag{23}$$

This expression provides a zero value of parity splitting for the rotational band of a nucleus with rigid octupole deformation. The experimental and calculated values of the parity splitting in the ground state and the first negative parity bands of ^{240}Pu are shown in Fig. 4. Having maximum value in the beginning of the band, the parity splitting decreases with increasing angular momentum. The reason for this is the following. The moment of inertia of the mononucleus is sufficiently smaller than the rigid body moment of inertia. Due to this fact, the energies of the cluster configurations decrease with respect to the energies of the mononucleus with increasing angular momentum. As a result, the average mass asymmetry increases with angular momentum as well. The behavior of the mass asymmetry with angular momentum for different rotational bands is illustrated in Table II. According to Eq. (5) the barrier between left and right positions of the light cluster with respect to the heavy one increases with mass asymmetry. Thus, the motion of the

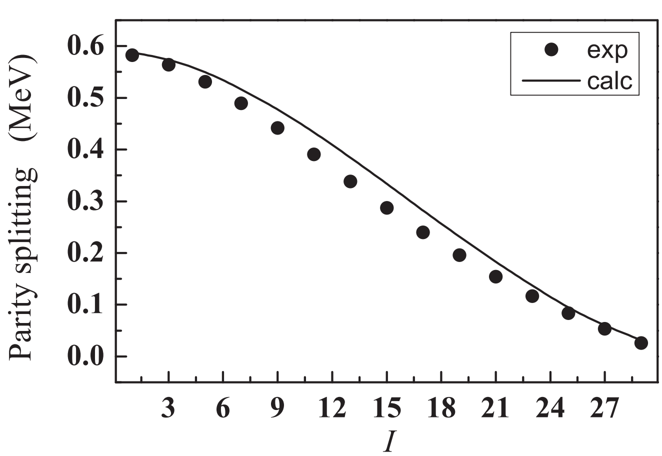

FIG. 4. Calculated (lines) and experimental (points) values of parity splitting for ^{240}Pu [see Eq. (23)]. Experimental values are taken from the data of Ref. [32].

TABLE II. Calculated average mass asymmetry $\overline{\xi}$ for the members of the ground-state band A, the second excited positive parity band D, and the lowest negative-parity band B in ^{240}Pu.

$I^+_{A,D}$	$\overline{\xi}_A$	$\overline{\xi}_D$	I^-_B	$\overline{\xi}_B$
0	0.196	0.396	1	0.333
2	0.197	0.397	3	0.335
4	0.200	0.400	5	0.338
6	0.203	0.404	7	0.343
8	0.209	0.410	9	0.350
10	0.215	0.417	11	0.359
12	0.224	0.426	13	0.369
14	0.235	0.435	15	0.381
16	0.247	0.445	17	0.394
18	0.263	0.455	19	0.409
20	0.282	0.464	21	0.425
22	0.305	0.469	23	0.442
24	0.333	0.474	25	0.459
26	0.367	0.473	27	0.478
28	0.407	0.469	29	0.498
30	0.453	0.464		

system changes from the limit in which heavy fragment and light fragments rotate almost independently of each other to the limit in which the light fragment is localized at the pole of the heavy fragment. In the former case, which is realized for large angular momenta, the motion can be approximated as the rotation of the nucleus with stable reflection-asymmetric deformation.

C. Multipole transitions

With the wave functions obtained one can find the reduced transition matrix elements of the electric dipole and quadrupole moments defined in Eqs. (14). The results are summarized in Tables III and IV. The effective charge for $E2$ transitions is set to be unity, $\epsilon_2 = e$. For the $E1$ transition, the effective charge is taken as $\epsilon_1 = 0.1e$. The reason to introduce this renormalization is the following. As seen from Eqs. (14), the results for the absolute values of the electric dipole moment are sensitive to the difference in Z/A ratios of the fragments. In the present calculations we do not consider the charge asymmetry as an independent coordinate. Instead, we take the Z/A ratio in the light fragment equal to 0.5 as in the α particle. This consideration is, of course, oversimplified and requires the introduction of the effective charge.

The calculated reduced matrix elements for the quadrupole transitions are listed in Table III. The quadrupole moment weakly depends on angular momentum. The quadrupole operator is a sum of two terms. Even for the pure cluster system, the dominate term of the quadrupole moment is generated by the strongly deformed heavy fragment while the presence of the light fragment gives only a small correction. Due to this fact, the quadrupole moment for the pure mononucleus is almost the same as for the pure cluster system with an α particle. Thus, even though the relative weights of the mononucleus and α-particle cluster system vary, the quadrupole moment remains almost the same.

TABLE III. Calculated $E2$-transition matrix elements $\langle I^+_A \| E2 \| (I+2)^+_A \rangle$ and $\langle I^+_D \| E2 \| (I+2)^+_D \rangle$ between the members of the ground-state band A and excited reflection asymmetric positive parity band D, respectively, and the matrix elements $\langle I^+_A \| E2 \| (I+2)^+_D \rangle$ of the interband transitions in ^{240}Pu.

I	$\langle I^+_A \|\| E2 \|\| (I+2)^+_A \rangle$ (e b)	$\langle I^+_D \|\| E2 \|\| (I+2)^+_D \rangle$ (e b)	$\langle I^+_A \|\| E2 \|\| (I+2)^+_D \rangle$ (e b)
0	3.905	4.131	0.075
2	6.264	6.630	0.086
4	7.904	8.375	0.069
6	9.254	9.821	0.037
8	10.434	11.094	0.004
10	11.499	12.252	0.050
12	12.483	13.328	0.100
14	13.408	14.338	0.158
16	14.290	15.291	0.224
18	15.144	16.186	0.310
20	15.978	17.018	0.419
22	16.823	17.776	0.588
24	17.675	18.449	0.837
26	18.565	19.051	1.093
28	19.498	19.577	1.356

Another consequence of the fact that the quadrupole moment weakly depends on the mass asymmetry is the suppression of the interband transitions. Our calculations suggest that the band D is built on the first excited state in ξ. Therefore, the quadrupole transitions from the band D to the ground state band A are expected to be weak. The reduced matrix elements for these transitions are presented in the last column of the Table III. The matrix elements for the interband transitions are almost two orders of magnitude smaller than those for the intraband transitions.

The calculated reduced matrix elements of dipole transitions are listed in Table IV. Using the results of Table IV, we extract the dipole moment as a function of the angular momentum with the expression [3]

$$B(E1, I_i \to I_f) = \frac{1}{2I_i+1} |\langle I_i \| E1 \| I_f \rangle|^2 = \frac{3}{4\pi} \left(C^{I_f 0}_{I_i 0\, 10}\right)^2 D_0^2. \quad (24)$$

The results are shown in Fig. 5. The dipole moment is an increasing function of angular momentum. Our model suggests the following explanation of this effect. Due to different N/Z ratios in the fragments, the dipole moment for the α-particle cluster system is large (for the pure α-particle DNS, $D_0 \approx 4\, e$ fm). With increasing angular momentum the weight of the cluster configuration with an α particle increases as well as the dipole moment. As seen, at $I_i < 10$ the dipole moment for the transition between the ground-state band and the first negative parity band lies in the range $D_0 \approx (0.05\text{–}0.08)\, e$ fm. It increases with angular momentum and achieves the value $\sim 0.15\, e$ fm for $I_i > 20$. This result is in a good agreement

TABLE IV. Calculated $E1$-transition matrix elements $\langle I_A^+\|E1\|(I+1)_B^-\rangle$ between the members of the ground-state band A and the lowest negative-parity band B, and matrix elements $\langle I_D^+\|E1\|(I+1)_B^-\rangle$ between the members of excited positive parity band D and the band B in ^{240}Pu.

I_i^+	I_f^+	$\langle I_A^+\|E1\|(I\pm 1)_B^-\rangle$ (e fm)	$\langle I_D^+\|E1\|(I\pm 1)_B^-\rangle$ (e fm)
0	1	0.029	0.047
2	1	0.037	0.061
2	3	0.053	0.079
4	3	0.050	0.086
4	5	0.072	0.104
6	5	0.058	0.105
6	7	0.089	0.125
8	7	0.065	0.122
8	9	0.106	0.145
10	9	0.072	0.140
10	11	0.123	0.163
12	11	0.080	0.160
12	13	0.141	0.181
14	13	0.089	0.182
14	15	0.160	0.197
16	15	0.102	0.207
16	17	0.181	0.211
18	17	0.117	0.233
18	19	0.206	0.223
20	19	0.138	0.260
20	21	0.233	0.232
22	21	0.165	0.285
22	23	0.265	0.235
24	23	0.199	0.307
24	25	0.302	0.233
26	25	0.243	0.323
26	27	0.344	0.223
28	27	0.297	0.330
28	29	0.391	0.203
30	29	0.360	0.325

with the experiment which suggests $D_0 \sim 0.2$ e fm for $I \geqslant 21$ [30].

For ^{240}Pu, the calculated D_0/Q_0 ratio is presented in Fig. 6. One can see a good agreement with the available experimental data [30]. It is worth noting that our model predicts strong increase of D_0/Q_0 ratio at $I_i \geqslant 21$. It is presently hard to confirm this prediction because of the large experimental error bars at large angular momentum.

As seen in Fig. 5, the dependence of the dipole moment on angular momentum demonstrates a staggered behavior. The dipole moment for the transition from state I of the ground-state band A to state $(I+1)$ of the first negative parity band B is generally larger than for the transition to state $(I-1)$ of band B. To understand the reason of this staggering, we use the approximate expressions for the wave functions of various bands (21). The basis functions (8), which mostly contribute to the state I_A, have an angular part $[Y_{l_1=I}(\Omega_h)\times Y_{l_2=0}(\Omega_R)]_{I_A M_A}$. For the states $(I+1)_B$ and $(I-1)_B$ of band B, the angular parts of the wave

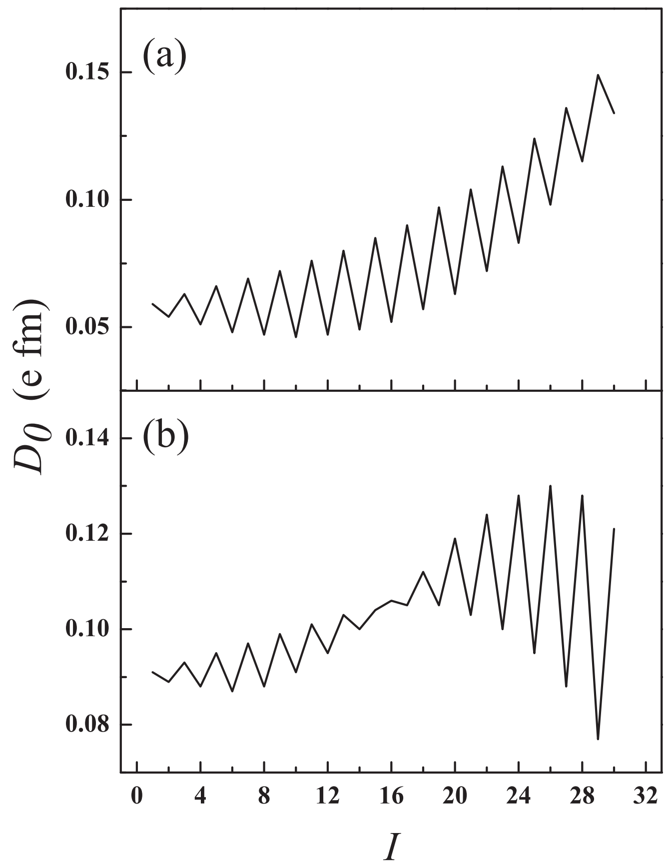

FIG. 5. Transition dipole moment D_0 for the transitions between the first negative-parity band B and the ground-state band B (a), and between the first negative parity band and the second excited 0^+ band D (b) as a function of the initial spin I.

functions are mainly defined by $[Y_{l_1=I}(\Omega_h)\times Y_{l_2=1}(\Omega_R)]_{I+1\,M}$ and $[Y_{l_1=(I-2)}(\Omega_h)\times Y_{l_2=1}(\Omega_R)]_{I-1\,M}$, respectively. As follows from expression (14), the dipole operator cannot change the angular momentum of the heavy fragment. Thus, the transition $I_A \to (I-1)_B$ is hindered.

With increasing angular momentum the structure of the states becomes more complicated. For example, at $I \geqslant 15$ the contribution of the basis states $[Y_{l_1=(I-2)}(\Omega_h)\times Y_{l_2=2}(\Omega_R)]_{I_A M_A}$ to the wave functions of the ground-state band cannot be neglected. Because of this, the hindrance mechanism described loses its significance. As seen in Fig. 5(a), the staggering of D_0 decreases at large values of angular momentum. One can expect that with further increase of angular momentum the spectrum approaches its rotational limit (see Appendix) and the staggering completely disappears.

The role of the structure of the wave functions is even more pronounced in the behavior of the dipole moment extracted from the reduced matrix elements $\langle I_D^+\|E1\|(I\pm 1)_B^-\rangle$ for the $E1$ transitions from the 0^+ band D to the first negativeparity band B. This behavior is illustrated in Fig. 5(b). The structure of the band D is more complicated than the structure of the ground-state band. Even in the beginning of the band the contribution of the basis function $[Y_{l_1=(I-2)}(\Omega_h)\times Y_{l_2=2}(\Omega_R)]_{I_D M_D}$ is important. Thus, for small

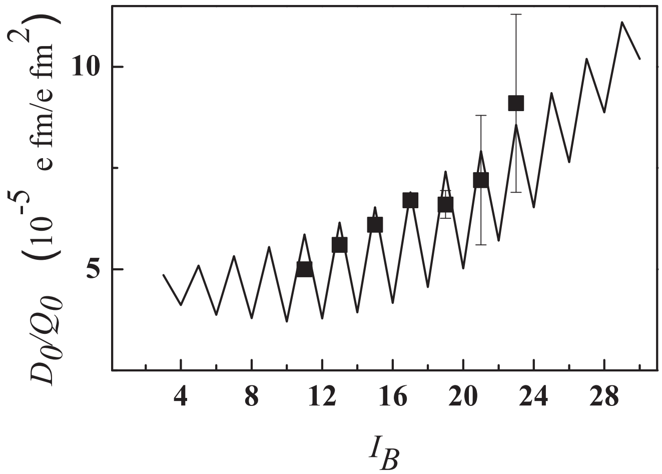

FIG. 6. Ratio of transition dipole and quadrupole moments extracted from the $E1$ and $E2$ branching ratio $B(E1,I_B^- \to (I-1)_A^+)/B(E2,I_B^- \to (I-2)_B^-)$ as a function of I_B. The experimental results are extracted from Ref. [30].

angular momentum the staggering of D_0 is weak. However, with increasing angular momentum the staggering starts to grow and change its pattern. From the approximate wave functions (21) it is clear that this staggering appears due to the contribution of the basis state $[Y_{l_1=(I-3)}(\Omega_h) \times Y_{l_2=3}(\Omega_R)]_{I_B M_B}$ to the wave function of the band B at large angular momenta.

In Table IV, the calculated values of the reduced matrix elements $\langle I_D^+ \| E1 \| (I-1)_B^- \rangle$ and $\langle I_A^+ \| E1 \| (I+1)_B^- \rangle$ are similar. This is in a good agreement with the experimental observations [31]. In this experiment, the branching ratios $B(E1)/B(E2)$ were measured between the $E1$ transition from band D to tband B and the $E2$ transition in band D. It was found that the $E1$ transitions linking bands D and B are similar to those linking bands B and A. The $B(E1)/B(E2)$ branching ratios between out-of-band and in-band transitions are of the same magnitude within the error bars. The results presented in Ref. [31] provide the value $D_0 \geqslant 0.2$ e fm for $I > 25$ both for transitions linking bands D and B and for transitions linking bands B and A. In our calculations, we obtain $D_0 \sim (0.13–0.16)$ e fm, which agrees well with the experimental data.

In the recent experiment [29], the branching $B(E1,I_D \to I_B)/B(E2,I_D \to I_A)$ ratios were investigated for the transitions to the negative parity band B and to the ground-state band. As seen in the Table V, the calculated results are in overall agreement with the experimental data. The values of $B(E1,I_D \to I_B)/B(E2,I_D \to I_A)$ are of the order of $\sim 10^{-6}$ fm^{-2}, which is significantly larger than the branching ratios $B(E1,I_B \to I_A)/B(E2,I_{B_i} \to I_{B_f}) \sim 10^{-9}$ fm^{-2} even at large spins. The reason for this is that the interband $E2$ transitions $I_D \to I_A$ are strongly suppressed.

V. SUMMARY

We suggested the cluster interpretation of the properties of multiple negative parity bands in deformed even-even actinides. The collective motion related to the cluster degree of freedom leads to the admixture of very asymmetric cluster configurations to the intrinsic nucleus wave function. To take into account the reflection asymmetric modes with $K \neq 0$, the rotational excitations of the heavy cluster are taken into account. The resulting energy spectrum consists of the ground state band, the excited 0^+ band, and several negative parity rotational bands which can be interpreted as $K^\pi = 0^-$ and $K^\pi = 1^-$ bands. As an example, ^{240}Pu was treated. The angular momentum dependence of the parity splitting is well described. The results of calculations support the cluster feature of low-lying negative parity states and some excited 0^+ bands. Comparing with our previous calculations for ^{220}Th [37], we note the weak variation of the parameters of the model. So, the predictive power of the cluster approach seems to be quite high.

TABLE V. Calculated $r_{\text{calc.}} = B(E1,I_D \to I_B)/B(E2,I_D \to I_A)$ ratios are compared with the experimental values ($r_{\text{exp.}}$) for the low-spin members of the $K^\pi = 0_2^+$ rotational band in ^{240}Pu. The experimental values are taken from Ref. [29].

I_D^π	$I_{B,E1}^\pi$	$I_{A,E2}^\pi$	$r_{\text{exp.}}$ (10^{-6} fm^{-2})	$r_{\text{calc.}}$ (10^{-6} fm^{-2})
0_2^+	1_1^-	2_1^+	13.7(3)	16.64
2_2^+	1_1^-	0_1^+	99(15)	66.92
2_2^+	1_1^-	2_1^+	26(2)	30.73
2_2^+	1_1^-	4_1^+	5.9(3)	8.14
2_2^+	3_1^-	0_1^+	149(22)	110.94
2_2^+	3_1^-	2_1^+	39(2)	50.99
2_2^+	3_1^-	4_1^+	8.9(5)	13.50
4_2^+	3_1^-	6_1^+	4.4(11)	6.97
4_2^+	5_1^-	6_1^+	4.7(13)	10.29

ACKNOWLEDGMENTS

This work was supported by the RFBR (Russian Federation) and NSFC (Beijing). T.M.S. acknowledges support from a CAS Fellowship for Young International Scientists (2013Y1JA0003) and the Russian Government Subsidy Program of the Competitive Growth of Kazan Federal University. S.G.Z. was partly supported by the 973 Program of China (Grant No. 2013CB834400), the NSF of China (Grants No. 11121403, No. 11120101005, and No. 11275248), and the Chinese Academy of Sciences (Grant No. KJCX2-EW-N01).

APPENDIX: BENDING MOTION

Let us consider the case of fixed mass asymmetry ξ_0. This corresponds to the potential in mass asymmetry with an infinitely deep minimum at $\xi = \xi_0$. The angular part of the Hamiltonian (7) is

$$H = \frac{\hbar^2}{2\Im_h} l_1^2 + \frac{\hbar^2}{2\mu R_{\text{m}}^2} l_2^2 + U_\epsilon(\xi_0)\left(\frac{2}{3} - \frac{8\pi}{3\sqrt{5}}[Y_2(\theta_1,\phi_1) \otimes Y_2(\theta_2,\phi_2)]_{00}\right). \quad \text{(A1)}$$

In the case of large $U_\epsilon(\xi_0)$, the problem is reduced to the rotation of the DNS system as a whole and the angular oscillations of the light cluster around its equilibrium position at the pole of the heavy cluster (so-called bending oscillations). The potential energy has a shape of two deep minima divided by the high barrier. Neglecting the penetration of the barrier, we can consider the oscillations in the vicinities of $\epsilon = 0$ and $\epsilon = \pi$ independently. The two states related to these values are degenerate and the states of correct parity are constructed as a superposition of these two states. Thus, in this approximation the parity splitting is zero. The Hamiltonian of bending motion can be rewritten in terms of Euler angles $\Omega = (\theta_1,\theta_2,\theta_3)$ of the DNS rotation as a whole and the bending angle ϵ as follows ($\sin\epsilon \approx \epsilon$ or $\sin\epsilon \approx \pi - \epsilon$):

$$\begin{aligned} H &= H_{\rm rot} + H_{\rm bend} + V_{\rm int},\\ H_{\rm rot} &= \frac{\hbar^2}{2\mu R_{\rm m}^2}(L^2 - 2L_3'),\\ H_{\rm bend} &= \frac{\hbar^2}{2\Im_b}\frac{1}{\epsilon}\frac{\partial}{\partial\epsilon}\epsilon\frac{\partial}{\partial\epsilon} + \frac{\hbar^2}{2\Im_b\epsilon^2}L_3'^2 + \frac{C}{2}\epsilon^2,\\ V_{\rm int} &= \frac{\hbar^2}{2\mu R_{\rm m}^2}\left[\frac{1}{\epsilon}(L_1'L_3' + L_3'L_1') + 2iL_2'\frac{1}{\sqrt{\epsilon}}\frac{\partial}{\partial\epsilon}\sqrt{\epsilon}\right], \end{aligned} \tag{A2}$$

with $\Im_b = \frac{\Im_h \mu R_{\rm m}^2}{\Im_h + \mu R_{\rm m}^2}$. Neglecting $V_{\rm int}$, the problem is analytically solved and

$$\begin{aligned} \Psi_{n,L,M,K} &= D^L_{MK}(\theta_1,\theta_2,\theta_3)L_{n,|K|}\big(\epsilon^2/\epsilon_0^2\big),\\ E_{L,M,K,n} &= \frac{\hbar^2}{2\mu R_{\rm m}^2}[L(L+1) - 2K^2] + \frac{\hbar^2}{\Im_b\epsilon_0^2}(2n + |K| + 1), \end{aligned} \tag{A3}$$

where $\epsilon_0^2 = \hbar/\sqrt{C\Im_b}$. Without $V_{\rm int}$ we get incorrect dependence of energy on K. Because $U_\epsilon(\xi_0) \gg 1$ or $\epsilon_0 \ll 1$, the $V_{\rm int}$ can be taken into account up to the zero order of ϵ_0. The corresponding correction provides

$$\begin{aligned} \Psi_{n,L,M,K} &= \sum_{k=K-2}^{k=K+2}\sum_n a(n,k)D^L_{M,k}(\theta_1,\theta_2,\theta_3)L_{n,|k|}\big(\epsilon^2/\epsilon_0^2\big),\\ E_{L,M,K,n} &= \frac{\hbar^2}{2\big(\Im_h + \mu R_{\rm m}^2\big)}(L(L+1) - K^2)\\ &\quad + \frac{\hbar^2}{\Im_b\epsilon_0^2}(2n + |K| + 1). \end{aligned} \tag{A4}$$

The moment of inertia is now given as a total moment of inertia and K becomes an approximate quantum number. The rotation energy correctly depends on K. So, in the limit of stable reflection asymmetric deformation, the excitation spectra of the model Hamiltonian (7) is represented as a sequence of rotational bands built upon the vibrational states with given n and K values.

[1] F. Asaro, F. S. Stephens, Jr., and I. Perlman, Phys. Rev. **92**, 1495 (1953).
[2] F. S. Stephens, Jr., F. Asaro, and I. Perlman, Phys. Rev. **100**, 1543 (1955).
[3] P. A. Butler and W. Nazarewicz, Rev. Mod. Phys. **68**, 349 (1996).
[4] I. Ahmad and P. A. Butler, Annu. Rev. Nucl. Part. Sci **43**, 71 (1993).
[5] V. M. Strutinsky, At. Energiya **4**, 150 (1956).
[6] K. Lee and D. R. Inglis, Phys. Rev. **108**, 774 (1957).
[7] W. Nazarewicz *et al.*, Nucl. Phys. A **429**, 269 (1984).
[8] P. Möller *et al.*, At. Data Nucl. Data Tables **94**, 758 (2008).
[9] J. Egido and L. Robledo, Nucl. Phys. A **494**, 85 (1989).
[10] K. Rutz, J. A. Maruhn, P.-G. Reinhard, and W. Greiner, Nucl. Phys. A **590**, 680 (1995).
[11] L. M. Robledo and G. F. Bertsch, Phys. Rev. C **84**, 054302 (2011).
[12] K. Wildermuth and Y. C. Tang, *Unified Theory of the Nucleus* (Academic, New York, 1977).
[13] W. D. M. Rae, Int. J. Mod. Phys. A **3**, 1343 (1988).
[14] M. Freer and A. C. Merchant, J. Phys. G **23**, 261 (1997).
[15] W. Nazarewicz, J. X. Saladin *et al.*, Phys. Lett. B **322**, 304 (1994).
[16] S. Åberg and L.-O. Jonsson, Z. Phys. A **349**, 205 (1994).
[17] T. M. Shneidman, G. G. Adamian, N. V. Antonenko, S. P. Ivanova, and W. Scheid, Nucl. Phys. A **671**, 119 (2000).
[18] T. M. Shneidman, G. G. Adamian, N. V. Antonenko, R. V. Jolos, and W. Scheid, Phys. Rev. C **67**, 014313 (2003).
[19] F. Iachello and A. D. Jackson, Phys. Lett. B **108**, 151 (1982).
[20] M. Gai *et al.*, Phys. Rev. Lett. **51**, 646 (1983).
[21] H. Daley and F. Iachello, Phys. Lett. **131**, 281 (1983).
[22] H. Daley and J. Barret, Nucl. Phys. A **449**, 256 (1986).
[23] B. Buck, A. C. Merchant, and S. M. Perez, Phys. Rev. C **59**, 750 (1999).
[24] B. Buck, A. C. Merchant, M. J. Horner, and S. M. Perez, Phys. Rev. C **61**, 024314 (2000).
[25] G. G. Adamian, N. V. Antonenko, R. V. Jolos, and T. M. Shneidman, Phys. Rev. C **70**, 064318 (2004).
[26] T. M. Shneidman, G. G. Adamian, N. V. Antonenko, and R. V. Jolos, Phys. Rev. C **74**, 034316 (2006).
[27] L. P. Gaffney *et al.*, Nature (London) **497**, 199 (2013).
[28] http://www.nndc.bnl.gov/ensdf
[29] M. Spieker *et al.*, Phys. Rev. C **88**, 041303(R) (2013).
[30] I. Wiedenhover *et al.*, Phys. Rev. Lett. **83**, 2143 (1999).
[31] X. Wang *et al.*, Phys. Rev. Lett. **102**, 122501 (2009).
[32] B. Singh and E. Browne, Nucl. Data Sheets **109**, 2439 (2008).
[33] R. V. Jolos, P. von Brentano, and R. F. Casten, Phys. Rev. C **88**, 034306 (2013).
[34] N. Minkov, S. Drenska, K. Drumev, M. Strecker, H. Lenske, and W. Scheid, Phys. Rev. C **88**, 064310 (2013).
[35] Ch. Briancon and I. N. Mikhailov, in *Proceedings of the International Conference on Nuclear Structure, Reactions and Symmetries*, edited by R. A. Meyer and V. Paar (World Scientific, Singapore, 1986), Vol. 1, p. 131.
[36] S. Frauendorf, Phys. Rev. C **77**, 021304(R) (2008).
[37] T. M. Shneidman, G. G. Adamian, N. V. Antonenko, R. V. Jolos, and W. Scheid, Eur. Phys. J. A **47**, 34 (2011).

[38] W. Reviol *et al.*, Phys. Rev. C **74**, 044305 (2006).
[39] B.-N. Lu, E.-G. Zhao, and S.-G. Zhou, Phys. Rev. C **85**, 011301(R) (2012).
[40] B.-N. Lu, J. Zhao, E.-G. Zhao, and S.-G. Zhou, Phys. Rev. C **89**, 014323 (2014).
[41] G. G. Adamian, N. V. Antonenko, and W. Scheid, in *Clusters in Nuclei*, edited by Ch. Beck, Lecture Notes in Physics 848 (Springer-Verlag, Berlin, 2012), Vol. 2, p. 165.
[42] G. G. Adamian, N. V. Antonenko, and R. V. Jolos, Nucl. Phys. A **584**, 205 (1995).
[43] P. Möller, J. R. Nix, W. D. Myers, and W. J. Swiatecki, At. Data Nucl. Data Tables **59**, 185 (1995).
[44] G. Audi, O. Bersillon, J. Blachot, and A. H. Wapstra, Nucl. Phys. A **729**, 3 (2003).
[45] A. B. Migdal, *Theory of Finite Fermi Systems and Applications to Atomic Nuclei* (Wiley, New York, 1967).
[46] G. G. Adamian, N. V. Antonenko, R. V. Jolos, S. P. Ivanova, and O. Melnikova, Int. J. Mod. Phys. E **5**, 191 (1996).
[47] T. M. Shneidman, G. G. Adamian, N. V. Antonenko, R. V. Jolos, and S.-G. Zhou, J. Phys.: Conf. Ser. **569**, 012056 (2014).
[48] Y. S. Chen, Y. Sun, and Z. C. Gao, Phys. Rev. C **77**, 061305(R) (2008).
[49] J. Zhao, B.-N. Lu, E.-G. Zhao, and S.-G. Zhou, Phys. Rev. C **86**, 057304 (2012).
[50] R. V. Jolos and P. von Brentano, Phys. Rev. C **49**, R2301(R) (1994).